



Closed tubular mechanical metamaterial as lightweight load-bearing structure and energy absorber

Xueyan Chen ^{a,b}, Qingxiang Ji ^{a,b}, Julio Andrés Iglesias Martínez ^b, Huifeng Tan ^{a,*}, Gwenn Ulliac ^b, Vincent Laude ^b, Muamer Kadic ^{b,*}

^a National Key Laboratory of Science and Technology on Advanced Composites in Special Environments, Harbin Institute of Technology, 92 Xidazhi Street, Harbin, 150001, PR China

^b Institut FEMTO-ST, CNRS, Université Bourgogne Franche-Comté, 25030 Besançon, France

ARTICLE INFO

Keywords:

Mechanical metamaterial
Lightweight structure
Loading support
Energy absorption

ABSTRACT

Periodic truss-lattice materials, especially when combined with current additive manufacturing techniques, are attracting attention in lightweight material engineering. As a member of the elementary cubic truss family, the simple-cubic truss lattice possesses the highest stiffness and strength along the principal directions and plays an important role in load-bearing mechanical metamaterials. High anisotropic mechanical properties and low resistance to buckling loading and shearing loading, however, limit its use in energy absorption. Here, we present a class of simple-cubic closed tubular lattice with limited loading direction dependence along with high mechanical properties and irregular stable post-yield response. The fabrication of its complex structure was made possible by direct laser writing at the microscale. Experiments and simulations demonstrate that both the elastic modulus and the yield strength of the simple-cubic closed tubular lattice are significantly larger than those of the simple-cubic truss lattice, regardless of the loading direction. At a relative density of 0.1 and compared to the truss lattice, the closed tubular lattice can absorb respectively 4.45 times and 6.14 times as much energy along directions [100] and [110]. The average normalized Young's modulus and yield strength are respectively 28% and 53% larger than those of the most outstanding shellular metamaterial with the same mass. Such excellent mechanical properties make it a potential candidate for applications to load-bearing and energy absorption.

1. Introduction

During the last two decades, periodic lattice materials have attracted considerable attention due to their outstanding mechanical properties (Coulais et al., 2018; Florijn et al., 2014; Milton and Cherkaev, 1995; Schittny et al., 2014; Frenzel et al., 2019, 2017; Zhu et al., 2019; Tao et al., 2020; Tan et al., 2019C, 2020; Chen et al., 2020a,c, 2021) such as high specific stiffness (Berger et al., 2017), high specific strength (Chen et al., 2020b; Jang et al., 2013; Zheng et al., 2014), controlled Poisson's ratio (Bückmann et al., 2012; Chen et al., 2020d; Yang and Ma, 2020; Bückmann et al., 2014), high energy absorption and ability to recovery after unloading (Tan et al., 2019b,a; Frenzel et al., 2016; Jang et al., 2013). Early experiments performed by Deshpande et al. have shown that a well-designed periodic truss lattice material exhibits much higher mechanical properties than non-periodic structural materials of equal mass such as commercially available aluminum foams (Deshpande et al., 2001b). Thus, truss lattice materials are

* Corresponding authors.

E-mail addresses: tanhf@hit.edu.cn (H. Tan), muamer.kadic@univ-fcomte.fr (M. Kadic).

<https://doi.org/10.1016/j.jmps.2022.104957>

Received 22 July 2021; Received in revised form 30 March 2022; Accepted 27 May 2022

Available online 14 June 2022

0022-5096/© 2022 Elsevier Ltd. All rights reserved.

very promising, especially when combined with current additive manufacturing techniques such as selective laser melting or direct laser writing (DLW) (Deubel et al., 2004; Kadic et al., 2012; Chen et al., 2020d; Blasco et al., 2016).

As pointed out by Gibson and Ashby, the mechanical properties of truss lattice materials are determined by structural topology and geometrical parameters besides the base material (Gibson and Ashby, 1999). For instance, the stiffness and the strength of lattice materials that are governed by the bending of micro-components scale non-linearly with the relative density (with an exponent between 1.5 and 2), while for lattice materials that deform in stretching mode, both stiffness and strength are expected to scale linearly. Later, Deshpande et al. identified the topological criteria for dictating the deformation mechanism of truss lattice materials (Deshpande et al., 2001a). Henceforth, truss lattice materials can be topologically categorized as either bending-dominated or stretching-dominated.

As a member of the face-centered-cubic (FCC) family, octet truss lattice materials may be the most well-known stretching-dominated lattices. Deshpande et al. derived theoretical estimates for the effective mechanical properties of octet truss lattices under loading along the [100] direction (Deshpande et al., 2001b). Elsayed and Pasini investigated the effect of shaping the micro-strut cross-section on the structural performance of the octet lattice (Elsayed and Pasini, 2010). Their study clearly showed that shaping the cross-section of the strut could change the failure mode of the low relative density octet lattice from buckling to plastic yield, therefore enhancing its strength. Later, Meza et al. experimentally verified the above theory by presenting a class of strong, lightweight, and recoverable three-dimensional ceramic hollow truss nanolattices (Meza et al., 2014). Using a combination of classical molecular dynamics simulations and theoretical analysis, He et al. demonstrated that surface effects have little influence on the stiffness and the strength scaling of nanolattices (He et al., 2017). Tancogne et al. numerically determined the effect of the relative density and truss variations on the macroscopic compressive response of octet truss lattice materials (Tancogne-Dejean et al., 2016). Simulations demonstrated that the compression failure of metallic lattice materials is dominated by unstable twist rather than stable bending for relative densities smaller than 0.3, the opposite being true for relative densities larger than 0.3. The compressive response was revisited by Chen et al. both theoretically and experimentally (Chen and Tan, 2018). Their experiments clearly showed that the compressive response of an octet lattice material made from Duraform PA changed from unstable shearing mode to stable bending mode at a relative density between 0.22 and 0.23. Their experimental and theoretical results further showed that both the nodal effect and the bending and shearing effects increased the compressive stiffness and strength.

Body-centered-cubic (BCC) structures play an important role in bending-dominated lattice materials. Based on the Euler–Bernoulli beam theory, Ushijima et al. presented a theoretical model for predicting the compressive stiffness and the strength of BCC lattice materials (Ushijima et al., 2011). Using Timoshenko beam theory, Gümürük and Mines suggested a more satisfying theoretical method for all aspect ratio ranges (Gümürük and Mines, 2013). They pointed out that the shearing effect should be taken into account when the aspect ratio of the strut is larger than 0.1. Using the strain energy method, Tancogne et al. derived theoretical estimates for the three independent moduli of the BCC truss lattice (Tancogne-Dejean and Mohr, 2018b). Their numerical investigation revealed that the effective elastic modulus and the specific energy absorption respectively increase by about 70% and 45% by tapering the beam cross-section.

As defined by Zok et al. the simple-cubic (SC) lattice, together with the BCC lattice and the FCC lattice, constitute an elementary cubic truss family (Zok et al., 2016). In theory, the SC lattice should belong to the bending-dominated family. In fact, the SC lattice possesses the highest Young's modulus but the lowest shear modulus along the [100] direction within the elementary cubic family. High anisotropic mechanical properties and low resistance to buckling loading and shearing loading limit its application to energy absorption. A recent work on elastically-isotropic elementary cubic lattices has shown that tailoring the hollow beam could reduce anisotropy, however, at the expense of stiffness (Tancogne-Dejean and Mohr, 2018a).

According to theory, only closed-cell materials can attain the theoretical limit (Hashin–Shtrikman upper bounds) for isotropic mechanical properties (Christensen, 1986). Plate lattices (Berger et al., 2017; Tancogne-Dejean et al., 2018) may have been the earliest to achieve the theoretical upper bounds. Their unstable buckling nonlinear mechanical response, however, limits their use in energy absorption (Li et al., 2021). As an alternative to open-form tubular lattice and plate lattice, a new class of SC closed-form tubular lattice is proposed in this paper to overcome the above weaknesses, for energy absorption and load-bearing. Finite element simulations are performed to investigate the elastic moduli and the collapse strength of the proposed material for relative density ranging from 0.1 to 0.5. Numerical results show that the closed tubes lead to higher mechanical properties, reduced anisotropy, and significantly enhanced resistance to shearing and buckling loading, without affecting the stiffness. Uniaxial compressive experiments on micro lattices fabricated by two-photon lithography show that the designed metamaterial possessing stable nonlinear response outperforms truss and shellular cubic metamaterials of the same relative density.

2. Metamaterial design

For 3D lightweight load-bearing and energy absorbing material design, a crucial aspect is to make the best use of every part of the structure. Obviously, in the absence of weight constraints, the ideal candidate would be the homogeneous solid itself. However, when aiming at the design of a lightweight structure, one has to decrease the volume and thus to remove material or to create inner holes. Structural design therefore becomes the real playground for optimization.

Under uniaxial compression, a lightweight 2D SC frame generally exhibits a decreasing post-buckling response following the initial linear regime valid for small displacements, as depicted in Fig. 1A and B. Only the vertical strut supports loading, which is unreasonable from the design point of view. The mechanical behavior changes significantly when the plain struts are replaced with a closed tube. The force–displacement curves suggest that the tube possesses a slightly larger elastic stiffness but mostly a much

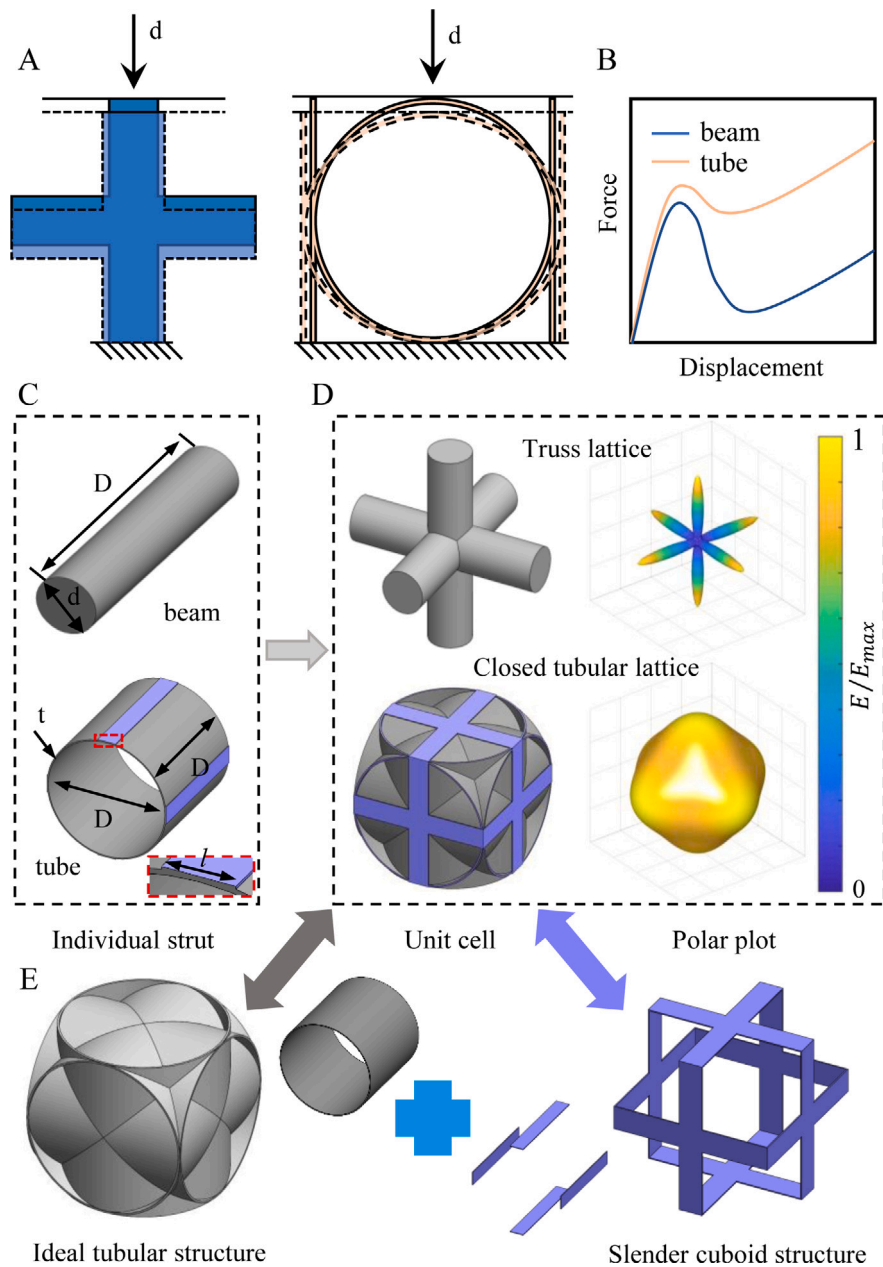


Fig. 1. Design concepts for tubular lattices. (A) Uniaxial compression mechanism for two dimensional simple cubic lattices composed of either solid beams or closed tubes. (B) Schematic force–displacement curves of a single unit cell show that the tubular lattice always exhibits higher elastic response and more stable nonlinear response compared to a truss lattice of the same relative density. Geometrical parameters for (C) individual struts (either beam or tube) and (D) the corresponding representative unit cell of an assembly. Polar plots depict the normalized Young’s modulus as a function of the loading direction. (E) General process to design novel tubular lattice structures from ideal tubular structure and slender cuboid structure which is used to avoid zero thickness errors in the 3D CAD software.

more stable nonlinear response. This may be attributed to the fact that the sides of the cylinder tube provide additional support under loading and resist the buckling strength, in contrast to struts.

This design idea also applies to the 3D case. Fig. 1C defines the relevant geometrical parameters. For a solid cylindrical strut of length L , the cross-section is circular with a constant diameter d . For a closed cylindrical tube of length L and diameter D , the thickness t allows controlling the relative density. The unit cells are shown in Fig. 1D. The unit cell for the truss lattice is composed of three intersecting struts. The unit cell for the tubular lattice is also composed of three intersecting tubes, but to avoid vanishing surface contacts between adjacent unit cells, a cuboid with constant length l and thickness t is added, with $l = 0.15D$. The design

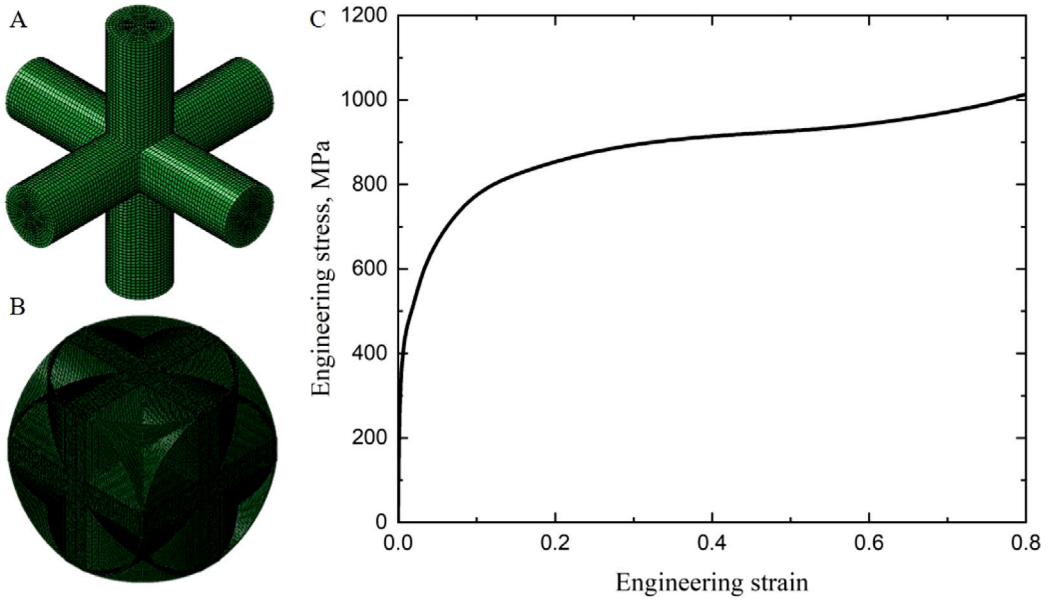


Fig. 2. Mesh model for (A) truss and (B) closed tubular lattices at a relative density of 0.1. (C) Engineering stress–strain curves for 316L stainless steel adopted in simulations.

procedure is detailed in the Supporting Information. The relative density ρ^* is defined as the ratio of the actual volume to the volume of the cubic unit cell and can be easily obtained via a 3D CAD software.

The anisotropy of lattice materials is a very important property. An energy absorbing material is indeed expected to display a similar mechanical behavior for all loading directions or at least to have no obvious weak directions, to avoid stress shielding. For example, from the polar plots in Fig. 1D we find that the SC truss lattice possesses a high stiffness in the principal directions but a much lower stiffness in all other directions. The SC tubular lattice is also, of course, anisotropic. Its anisotropy, however, is significantly reduced from $E_{\max}/E_{\min} = 14.36$ down to $E_{\max}/E_{\min} = 1.25$ compared to the truss lattice.

3. Numerical simulation

To identify the elastic moduli and yield strength of the SC lattice metamaterials, a series of unit cell models with relative density ranging from 0.1 to 0.5 were built using commercial software Abaqus. Truss lattices are meshed with first-order solid elements (type C3D8R) using at least seven elements along the radius of a beam. Due to their complex geometry, closed tubular lattices are built using quadratic tetrahedral elements (type C3D10). To ensure computation accuracy, we employ meshes with 80,784 elements for the truss lattice and 670,320 elements for the closed tubular lattice, as illustrated in Fig. 2A and B. For the same models with a relative density larger than 0.1, twice coarser meshes are adopted.

The basis material used in simulations is stainless steel 316L (SS316L). Such a homogeneous solid is modeled using an isotropic hardening elasto-plastic material model with a Young's modulus of 210 GPa and a Poisson's ratio of 0.3. The 0.2% offset yield strength is assumed to be 418 GPa. The detailed stress–strain response for stainless steel is depicted in Fig. 2C. For all models, the edge length of unit cells is fixed to 200 μm . The corresponding strut radius for the truss lattice and the wall thickness for the closed tubular lattice change with relative density. Periodic boundary conditions are applied by matching points for each pair of parallel unit-cell boundary surfaces with linear constraint equations.

Elastic simulations considering a small strain under uniaxial compression, pure shearing loading and hydrostatic compression along principal direction are conducted to extract Young's modulus, shear modulus and bulk modulus, respectively. Additional compression simulations up to a strain of -0.01 along 21 directions are performed to find extreme values for the yield strength of cubic symmetric lattices. The initial yield strength is defined by the axial stress at the point where the permanent strain is 0.2%.

3.1. Elastic properties

In the elastic region, the elastic anisotropy of cubic lattices is often quantified by Zener's ratio

$$Z = G \frac{9K - E}{3KE} \quad (1)$$

where G , K and E are respectively the shear modulus, the bulk modulus and Young's modulus of the lattice material in a principal direction. Elastic isotropy is achieved only when $Z = 1$. Fig. 3A illustrates the dependence of Zener's ratio with relative density

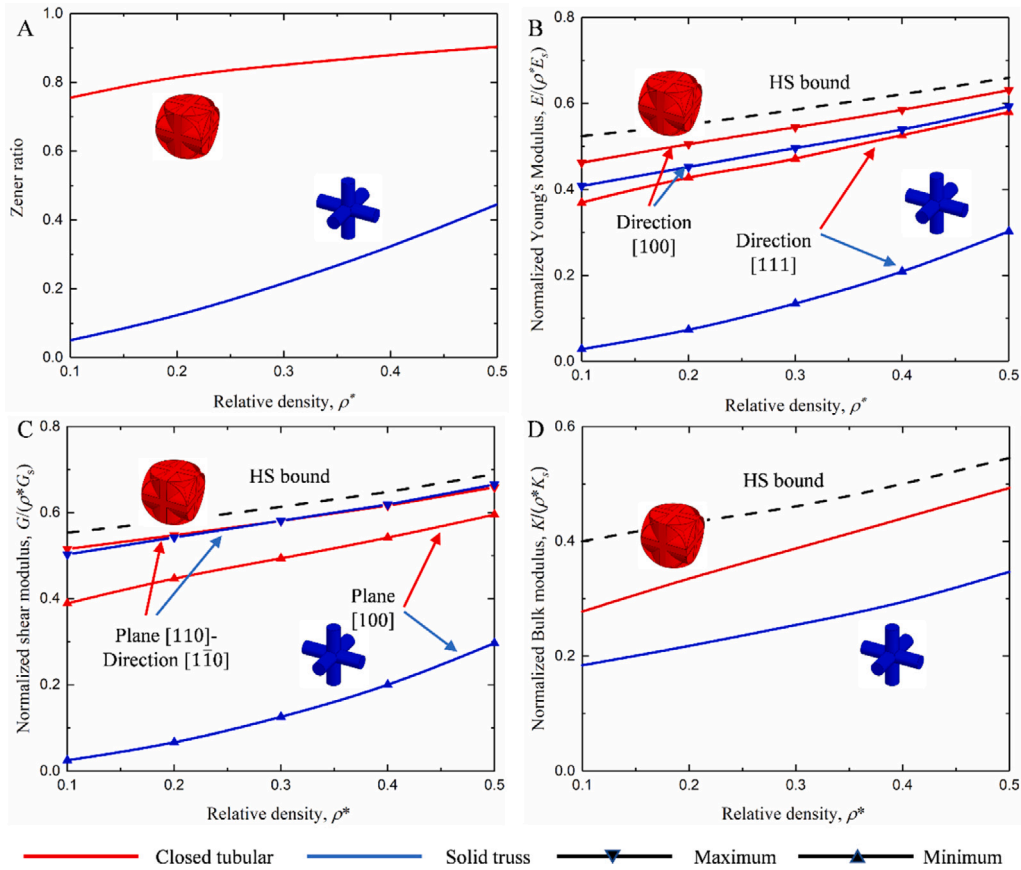


Fig. 3. Comparison of the elastic properties of simple-cubic closed tubular lattices and of truss lattices, as obtained from numerical simulation. (A–D) Evolution as a function of relative density of Zener’s ratio, of the normalized Young’s modulus, of the normalized shear modulus, and of the normalized bulk modulus.

for both the closed tubular lattice and the truss lattice; at a relative density of 0.1, $Z = 0.76$ for the former and $Z = 0.05$ for the latter. For both lattices, as the relative density increases, Zener’s ratio increases and would converge to 1 in the limit of the plain material. The influence of overlapping nodes as well as bending and shearing coupling deformation on anisotropy become more important as the relative density decreases, thus playing against lightweight lattices. It can also be observed that Zener’s ratio for the closed tubular lattice is always far larger than for the truss lattice. As a whole, the presence of the closed tube largely reduces the anisotropy of the SC lattice by redistributing the stress in a more uniform manner.

For cubic lattices, the directional dependence of Young’s modulus can be obtained as (Meyers and Chawla, 2008)

$$\frac{1}{E_{ijk}} = \frac{1}{E} - \frac{Z-1}{2G} \left(l_{i1}^2 l_{j2}^2 + l_{j2}^2 l_{k3}^2 + l_{i1}^2 l_{k3}^2 \right) \quad (2)$$

where E_{ijk} is Young’s modulus in the $[ijk]$ direction, and l_{i1} , l_{j2} and l_{k3} stand for the direction cosines of the $[ijk]$ direction vector with respect to the principal axes. Fig. 3B shows the evolution of the maximum and the minimum Young’s modulus as a function of the relative density, for both lattices. Hereafter, the effective mechanical properties of the metamaterial are normalized to those of the basis material and to the relative density, to allow a fair comparison. Both SC lattices exhibit their stiffest and softest uniaxial Young’s modulus respectively along directions $[100]$ and $[111]$. The stiffness of the closed tubular lattice is always larger than that of the truss lattice, regardless of the loading direction. The choice of loading direction has little influence on the stiffness of the closed tubular lattice, since it is always stretching dominated, while the opposite observation is true for the truss lattice: the stiffness of the truss lattice is stretching-dominated for $[100]$ direction loading and bending-dominated for $[111]$ direction loading. At a relative density of 0.1, the normalized stiffness of the truss lattice has a maximum of 0.41 and a minimum of 0.02. At the same relative density, the normalized stiffness of the closed tubular lattice is 1.12 times larger at the maximum and 18.5 times larger at the minimum. The normalized stiffness of the closed tubular lattice, whether in the maximum or the minimum direction, is very close to the theoretical limit for a plain solid. At a relative density of 0.5, the maximum and minimum values for the closed tubular lattice attain respectively almost 96% and 89% of the Hashin–Shtrikman (HS) bound.

The definition of the shear modulus requires to consider both the normal to the shear plane and the direction of shear. It is practical to consider a transformed coordinate system in which axis 3 is parallel to the normal of the shear plane and axis 2 is the

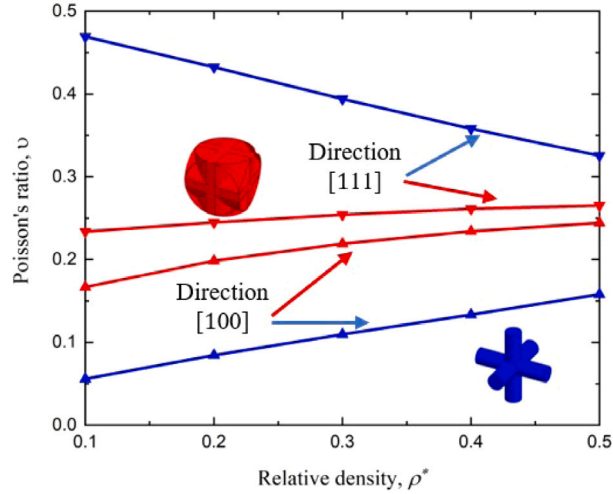


Fig. 4. Comparison of Poisson's ratio between closed tubular lattice and solid truss lattice, for the material SS316L.

direction of shear. The shear modulus can then be determined as (Knowles and Howie, 2015)

$$G_{ijk} = G \left(1 + 2 \left(\frac{1}{Z} - 1 \right) (a_{31}^2 a_{21}^2 + a_{32}^2 a_{22}^2 + a_{33}^2 a_{23}^2) \right) \quad (3)$$

where the a_{ij} are direction cosines specifying the angle between the i th axis of the transformed reference frame and the j th axis of the material reference frame. Figure S1C illustrates the scaling of the maximum and the minimum of the shear modulus as a function of the relative density, for both the closed tubular lattice and the truss lattice. The shear modulus generally increases with the relative density. Both lattices have their softest elastic shear modulus when either the shear direction is [100] or the shear plane is {100}. The lower limit for the closed tubular lattice is much larger than for the truss lattice. At a relative density of 0.1, the closed tubular lattice possesses a normalized shear modulus of about 0.39, almost 15.6 times as much as for the solid truss lattice, and almost reaches 71% of the HS bound. The stiffest elastic shear modulus is found on plane {100} when the shear direction is $[\bar{1}00]$, almost irrelevant of the choice of strut element. Both lattices have nearly the same extreme elastic shear response and attain about 93% of the HS bound even at relative densities as low as 0.1.

Fig. 3D depicts the variation of the bulk modulus as a function of the relative density for the closed tubular lattice and the truss lattice. The bulk modulus increases with the relative density for both lattices. It is noted that the closed tubular lattice exhibits a larger bulk modulus than the truss lattice; it is at least 1.5 times larger at a relative density of 0.1. Moreover, the closed tubular lattice reaches the HS bound faster than the truss lattice.

For cubic lattices, Poisson's ratio for arbitrary loading directions is calculated using formulas from our previous work (Chen et al., 2020d). Fig. 4 illustrates the maximum and the minimum Poisson's ratio for both configurations as a function of relative density. Extreme values for SC lattices are always found along directions [100] and [111]. Generally, Poisson's ratio increases with the relative density. However, the upper limit for the SC truss lattice decreases with the relative density. Moreover, the upper limit and the lower limit for the SC closed tubular lattice are very close to each other, especially when compared to its competitors. This provides further evidence of reduced anisotropy.

3.2. Yield strength

Figs. 5 and 6 compare the computed compressive responses of the truss lattice and the closed tubular lattice. While not isotropic, the closed tubular lattice exhibits a similar linear elastic behavior along the three high-symmetry directions for all relative densities considered. In contrast, the linear elastic response of the truss lattice is highly dependent on the loading direction, especially at low relative density. With regard to the subsequent nonlinear region of the compressive response, the closed tubular lattice still offers distinctive advantages over the truss lattice. The Von Mises stress distributions in Figure Fig. 5B–G clearly indicate that stress in the closed tubular lattice is distributed much more uniformly than in the truss lattice. As a result, the closed tubular lattice makes better use of its components than the truss lattice regardless of the loading direction.

The evolution of the relative yield strength as a function of relative density is summarized in Fig. 7. For the truss lattice, the strongest direction is [100], whereas the weakest direction is [110]. The yield strength distributions in the closed tubular lattice with relative densities of 0.1 and 0.2 are presented in Fig. 7(C,D). The maximum and minimum values are respectively found around directions [53,10,0] (as can be identified from the polar plot) and [100]. The yield strength of the closed tubular lattice is significantly larger than that of the truss lattice. Even in the worst case, when the loading direction is [100], the closed tubular lattice is stronger than the truss lattice. Fig. 7B displays the anisotropy of the yield strength. The relative density has little effect on the yield anisotropy of the closed tubular lattice: the yield strength ratio $\sigma_Y^{\max}/\sigma_Y^{\min}$ is almost constant and close to 1. In contrast, the

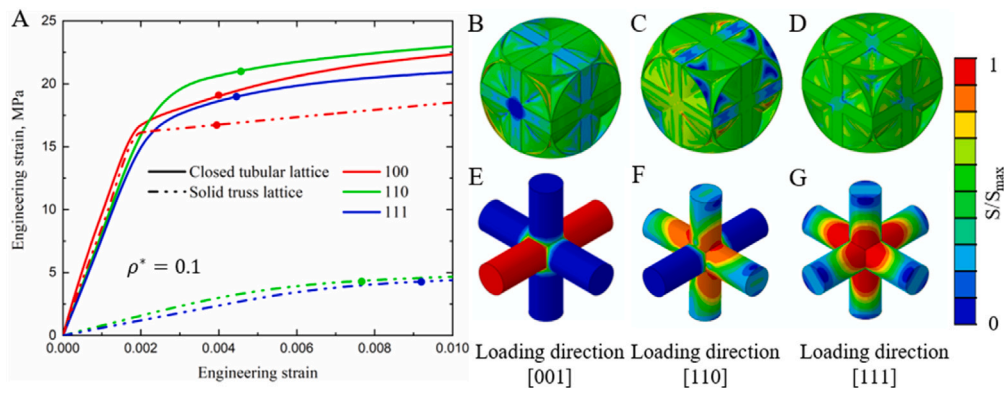


Fig. 5. (A) Engineering stress–strain curves for SC truss and closed tubular lattices at a relative density of 0.1, under uniaxial compression along directions [100], [110] and [111]. (B–G) Corresponding contour plots of the Normalized von Mises stress in closed tubular and truss lattices at a strain of 0.01. The material considered is SS316L.

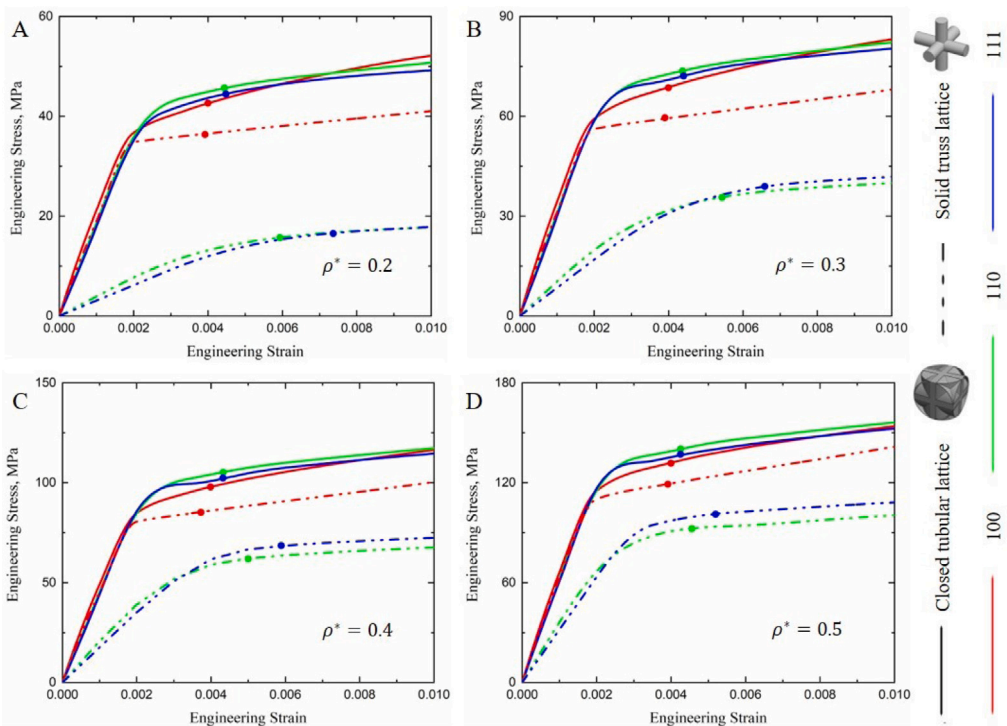


Fig. 6. (A–D) Compressive response of truss lattices and closed tubular lattices, with the relative density ranging from 0.2 to 0.5. The material considered is SS316L.

truss lattice possesses a much higher yield anisotropy. At a relative density of 0.1, the yield strength ratio $\sigma_c^{max}/\sigma_c^{min} \approx 4$. Anisotropy decreases as the relative density increases.

4. Experiments

Polymeric samples with $4 \times 4 \times 4$ unit cells were fabricated from the ‘IPS’ resin, using a 3D commercial printing system (Photonic Professional GT, Nanoscribe GmbH, Germany) with a speed of 100 mm/s and a laser power of 100 mW. Samples on top of fused silica substrates were developed via the polymerization of the liquid negative-tone photoresist. A subsequent 20 min PGMEA(1-methoxy-2-propanol acetate) bath is applied to remove the unexposed photoresist (see Supporting Information).

Two different configurations with relative densities 0.1 and 0.2 are considered in this work. For each configuration, two types of samples oriented along directions [100] and [110] were fabricated by dip-in DLW optical lithography in view of compression tests (see Fig. 8). All samples feature a unit cell length of 200 μm . For the SC truss lattice, relative densities of 0.1 and 0.2 are obtained

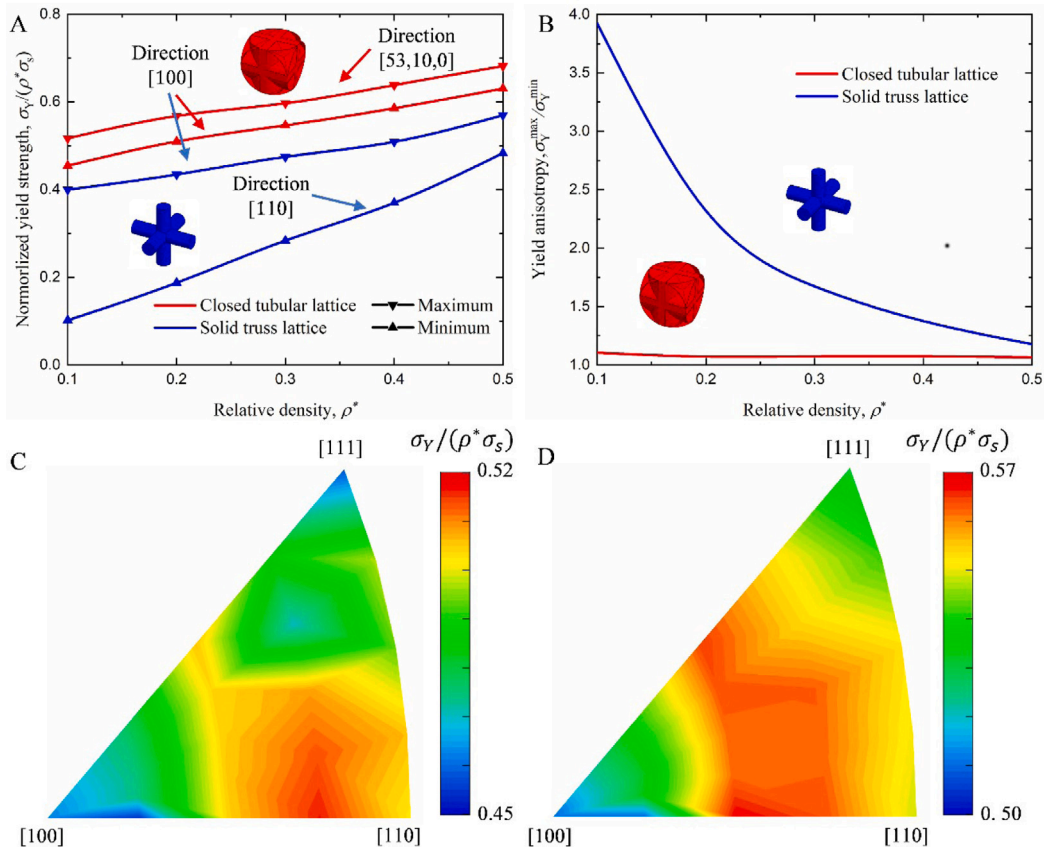


Fig. 7. (A) Normalized yield strength and (B) yield anisotropy of closed tubular and truss lattices as a function of relative density. Polar figures for yield strength distribution of the closed tubular lattice are shown with relative densities (C) 0.1 and (D) 0.2. Similar trends are observed at higher relative densities. The material considered is SS316L.

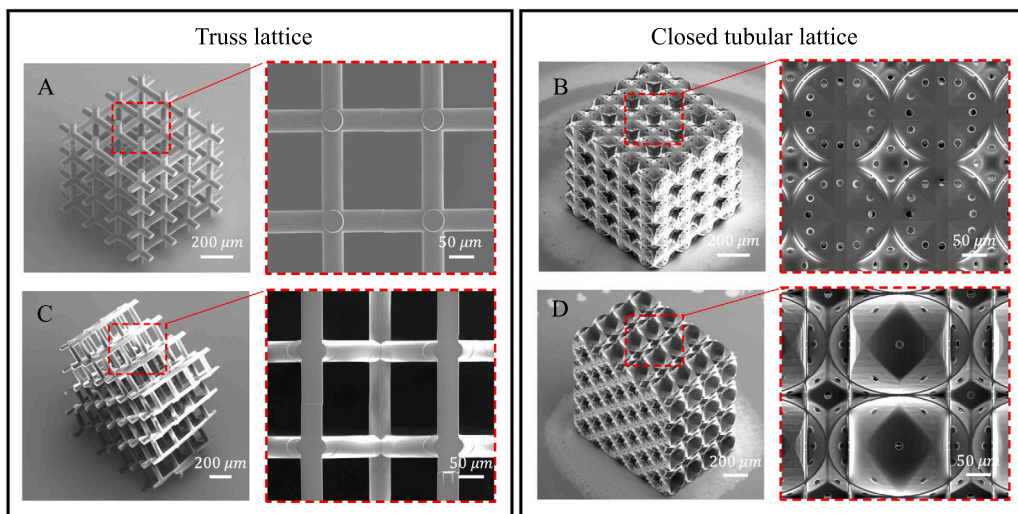


Fig. 8. SEM images of simple-cubic polymeric samples fabricated via 3D printing technology. Isometric views and zoom-in views are shown for truss and closed tubular lattices with relative density 0.1. (A) [100] truss lattice and (B) [100] closed tubular lattice. (C) [110] truss lattice and (D) [110] closed tubular lattice.

respectively for a strut diameter of 44.3 μm and 65 μm . For the SC closed tubular lattice, the tube thickness is respectively 2.3 μm and 5.1 μm . As a note, circular holes of a diameter of 15 μm had to be added at the center of each face to remove the unexposed resin (see

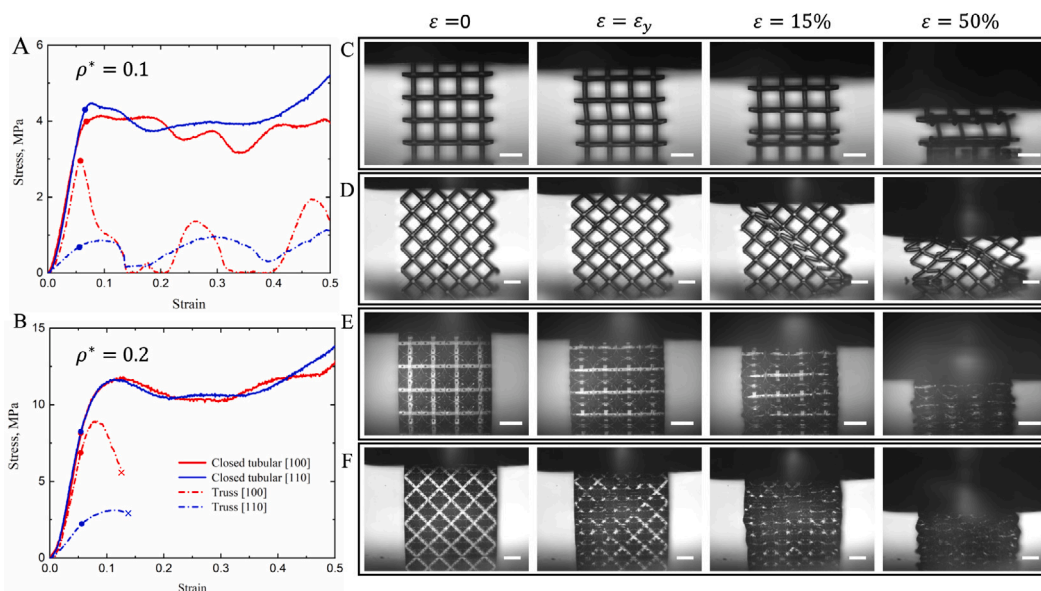


Fig. 9. Uniaxial compression experiments of SC [100] and [110] samples with different relative densities. Engineering stress–strain curves for the closed tubular and the truss lattices are shown for relative density (A) 0.1 and (B) 0.2. Photographs of the deformed samples during compression are shown for relative density 0.1 for (C) the [100] truss lattice, (D) the [110] truss lattice, (E) the [100] closed tubular lattice, and (F) the [110] closed tubular lattice. ϵ_y is the strain at the peak stress σ_y , or the experimental yield strength. All scale-bars are 200 μm long.

Supporting Information) (Tancogne-Dejean et al., 2018). Their effect of the holes on mechanical properties is almost insignificant, as detailed in the supplementary material.

Once fabricated, the polymeric microlattices were mechanically tested under uniaxial compression at a constant strain rate of 10^{-3} s^{-1} . Samples were placed between a fixed glass substrate and a flat loading device. The loading device equipped with a sensitive force sensor (Go Tronic model CZL616C or model CZL635-5) was driven by a brushless stepping motor (PI model M-404.42S, 200-nm resolution) and used to record the reacting force after analog to digital conversion (PhidgetBridge 4-input), see Fig.S5. The linear force sensor was calibrated using a set of standard masses. The position obtained directly from the linear stage was only used to monitor the fatigue of the material. Front-view videos of samples were used to monitor the deformation of the lateral faces and hence to correct the load and displacement curves via an in-house digital image correlation (DIC) algorithm (Eberl et al., 2006). For the $800 \mu\text{m} \times 800 \mu\text{m} \times 800 \mu\text{m}$ sample, the pixel resolution is about 550 nm per pixel, which insures the measurement precision. The Young's modulus was calculated based on the local axial strain measured from reference points at the central row of the unit cells (Fig.S2), and yield strengths were taken as the 0.2% offset strength of the engineering stress–strain curves.

5. Results and discussion

Fig. 9 illustrates the result of compressive experiments. Experimental stress–strain curves at a relative density of 0.1 are shown in Fig. 9A. The [100] truss lattice samples exhibit an almost linear elastic response followed by a brittle fracture at a stress of about 3 MPa. The peak stress is taken as the experimental yield strength ϵ_y in the following. The subsequent decrease of the response continues until the engineering strain reaches 0.15. At this point, the structure almost loses its loading capacity due to the catastrophic failure of sub-bottom layer struts (see Fig. 9C and Movie S1). The following oscillations of stress are caused by layers contacting and collapsing one after the other. In contrast, the catastrophic collapse mode of the [110] truss lattice sample is greatly reduced, as well as its compressive mechanical response. The brittle failure of struts along the diagonal direction is mainly affected by shearing forces rather than by nonlinear buckling (see Fig. 9D and Movie S2).

In the case of the closed tubular lattice samples, the mechanical response and the deformation mechanisms are completely different. For both directions [100] and [110], a nearly stable nonlinear response and a progressive failure are observed during compression (see Fig. 9E and F, and Movie S3 and S4). Deformations are more uniform compared to the truss lattice and slight oscillations arise from local buckling of the thin tubes. Similar trends were observed for all samples with the higher relative density 0.2 (see the stress–strain curves in Fig. 9B). The main difference is that truss lattice samples were completely crushed at an engineering strain of only 0.15. It may be attributed to the fact that struts with large diameters bear larger strength at low strain and are hence more sensitive to flaws and imperfections.

Table 1 summarizes the experimental values of Young's modulus, the yield strength and the specific energy absorption (SEA) of all test samples. At low relative density, Young's modulus and yield strength of the tubular lattice along the [100] direction are slightly larger than those of the truss lattice. In order to compare experiments and numerical simulations (see supplementary

Table 1
Mechanical data of the tested samples, including Young’s modulus, yield strength and specific energy absorption, for different configurations and different relative densities.

Specimens	Relative density	Direction	E (MPa)	σ_y (MPa)	SEA (J/g)
Truss lattice	0.1	[100]	97.76	2.95	4
		[110]	13.93	0.65	3.13
Tubular lattice	0.1	[100]	112.98	3.99	17.79
		[110]	111.13	4.3	19.21
Truss lattice	0.2	[100]	227.35	6.86	
		[110]	48.77	2.22	
Tubular lattice	0.2	[100]	249	8.13	25.13
		[110]	270	8.24	25.73

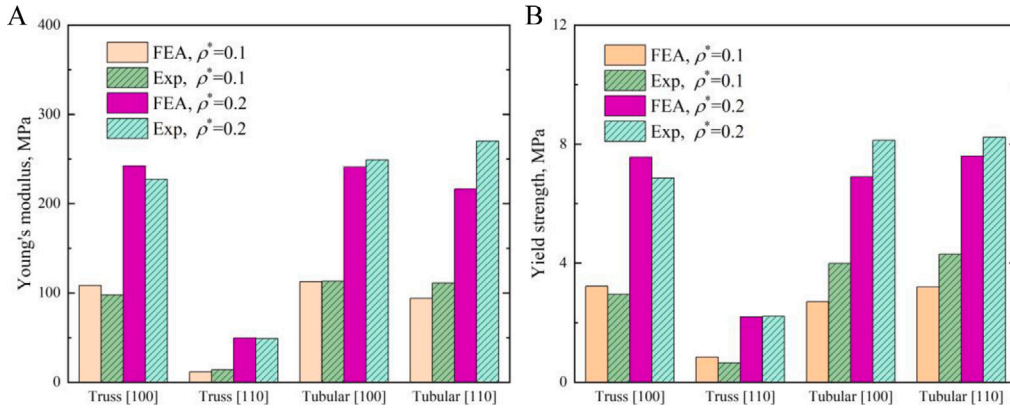


Fig. 10. Direct comparison of (A) Young’s modulus and (B) yield strength obtained in simulation and experiment.

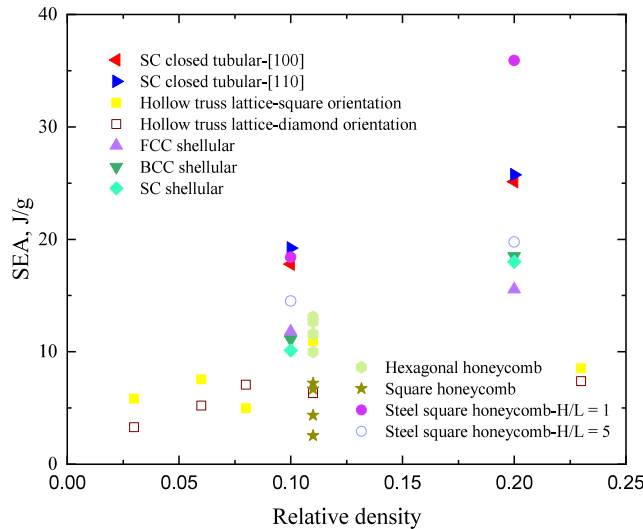


Fig. 11. Comparison of SEA between SC closed tubular samples in this paper and other efficient energy absorbers, including hollow truss lattice (Queheillat and Wadley, 2005), FCC shellular (Bonatti and Mohr, 2019), BCC shellular (Bonatti and Mohr, 2019), SC shellular (Bonatti and Mohr, 2019), hexagonal honeycomb (Duan et al., 2018), square honeycomb (Duan et al., 2018) and two sets of steel square honeycombs (Cote et al., 2004).

material and Fig. 10), elastic modulus and yield strength for tubular lattices and truss lattices are compared. Experimental results are in good agreement with numerical predictions in both directions [100] and [110]. Prediction errors maybe attributed to printing errors, imperfections and flaws. Truss lattices seem to be more sensitive to imperfections and flaws. In addition, unit cell simulations confined by periodic boundary conditions always provide an estimation that is stiffer than experiments with finite samples (Bonatti and Mohr, 2017). Moreover, the limited number of unit cells also reduces the elastic response of stretching-dominated materials with high stiffness (Bonatti and Mohr, 2017; Abueidda et al., 2017), whereas it has a limited influence on bending-dominated

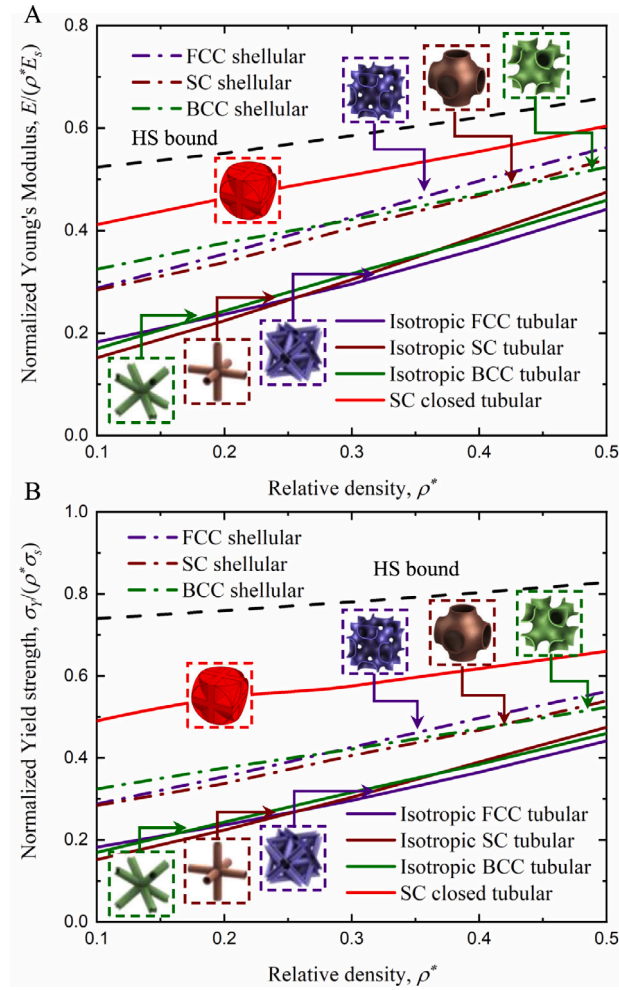


Fig. 12. Comparison of the mechanical properties of shellular and tubular lattices versus relative density. For a fair comparison, the average normalized (A) Young's modulus and (B) the yield strength of SC closed form tubular and other typical counterparts (Tancogne-Dejean and Mohr, 2018a; Bonatti and Mohr, 2019) are shown.

materials (Ushijima et al., 2011), which refers to the [110] truss lattice here. The opposite observation is true for the elastic–plastic phase. Therefore, deviations are expected to reduce when increasing the number of unit cells. Samples at higher relative density show similar trends. The SEA is defined as the work performed under uniaxial compression up to a strain of 0.5 per gram of mass as $SEA = \left(V \int_0^{0.5} \sigma d\varepsilon \right) / M$. At low relative density, the experimental value of SEA for the closed tubular lattice along the [100] direction and the [110] direction is respectively 4.45 times and 6.14 times larger than for the truss lattice. For a relative density of 0.2, absolute values $SEA = 25.13 \text{ J/g}$ and 25.73 J/g are found respectively for directions [100] and [110]. To support our conclusions, we further compared the SEA with other efficient energy absorbers, including hollow truss lattice (Queheillalt and Wadley, 2005), FCC shellular (Bonatti and Mohr, 2019), BCC shellular (Bonatti and Mohr, 2019), SC shellular (Bonatti and Mohr, 2019), hexagonal honeycomb (Duan et al., 2018), square honeycomb (Duan et al., 2018) and two sets of steel square honeycombs (Cote et al., 2004). The results are reported in Fig. 11. For all the relative densities considered, in terms of SEA, closed tubular lattices are similar to steel square honeycombs and are significantly better than other competing counterparts. For a relative density of 0.2, the IPS tubular lattice possesses a higher SEA than the steel square honeycomb for $H/L=5$, but a lower SEA for $H/L=1$. At low relative density, however, the IPS tubular lattice can absorb more impact energy than the steel square honeycomb for both $H/L=5$ and $H/L=1$. The tubular lattice is thus a potential alternative to the energy absorbers for low relative density.

Fig. 12 shows the dependence versus relative density of the average normalized Young's modulus and yield strength for the closed tubular lattice, compared with competing isotropic tubular lattices (Tancogne-Dejean and Mohr, 2018a) and shellular lattices (Bonatti and Mohr, 2019). Note that the lattices mentioned above are taken as representative of the tubular and the shellular families, especially for those lattices (Meza et al., 2014, 2017) with anisotropic elastic response. It is interesting to observe that both normalized elastic modulus and yield strength of the closed tubular lattice scale almost linearly with relative density. They can be approximated by the linear functions $E/(E_s \rho^*) = 0.365 + 0.475 \rho^*$ and $\sigma/(\sigma_s \rho^*) = 0.4 + 0.48 \rho^*$. Both elastic modulus and yield strength

are significantly larger than in the case of isotropic tubular lattices and shellular lattices, with a maximum advantage of 28% in stiffness and of 53% in strength at a relative density of 0.1. Concurrently, the modulus and strength of the SC closed tubular lattice reach respectively about 80% and 67% of their respective HS bound. These values become closer to the HS bound as the relative density increases. When the relative density is as large as 0.5, modulus and strength almost attain 92% and 81% of their respective HS bound. The underlying reasons for the outstanding mechanical behavior of the SC closed tubular lattice can be explained through a comparison with the open-form tubular lattice. As shown in Fig. S6, the SC open-form tubular lattice is taken as a representative of both tubular lattices and shellular lattices. First, under uniaxial compression, only the vertical strut of the open-form tubular lattice supports loading, which is unreasonable from the design point of view. In contrast, the closed-form tubular lattice makes better use of each component. Second, a larger radius always means a larger moment of inertia and a higher resistance to bending moment and shearing stress. Those are important reasons for the increase in both stiffness and strength. Third, there exist plenty of voids around the nodal connections of tubular and shellular lattices. These inherent weaknesses definitely weaken the mechanical performance, in terms of both stiffness and strength, and lead to stress concentration around nodes. In contrast, voids are completely avoided in the closed tubular lattice since three individual entire struts are directly combined. As a direct benefit of the incredibly stable mechanical response of cylindrical tubes, the resistance of the closed tubular lattice to buckling strength is further enhanced and recoverability is foreseeable by further reducing the thickness of the shell (Karathanasopoulos et al., 2020). As a whole, the combination of limited loading direction dependence, high specific stiffness, strength and irregular stable post-yield response make the closed tubular lattice a promising candidate for applications to hierarchical structures (Mizzi and Spaggiari, 2020; Dragoni and Ciace, 2019), load-bearing, as well as impact energy absorption.

6. Conclusion

Here, we have introduced a class of lightweight simple-cubic closed tubular lattice material possessing high specific stiffness, high specific strength and stable nonlinear response. Compared to the stiffest and strongest smooth shellular lattice and tubular lattice materials, for the same relative density, the gain in average stiffness and strength is respectively 28% and 53%. Experiments with samples fabricated by DLW optical lithography and simulations demonstrate that the replacement of solid struts with closed tubes largely reduces the elastic and the yield anisotropy of simple-cubic lattice materials. As a direct benefit of the incredibly stable mechanical response of cylindrical tubes, the resistance of the closed tubular lattice to buckling strength is further enhanced and recoverability is foreseeable by further reducing the thickness of the shell. This work provides a feasible pathway for applications in lightweight design, loading support, and impact energy absorption.

CRedit authorship contribution statement

Xueyan Chen: Conceptualization, Methodology, Software, Validation, Writing. **Qingxiang Ji:** Data curation, Validation. **Julio Andrés Iglesias Martínez:** Visualization, Validation. **Huifeng Tan:** Supervision, Writing. **Gwenn Ulliac:** Software, Validation. **Vincent Laude:** Writing, Supervision. **Muamer Kadic:** Writing, Supervision.

Declaration of competing interest

The authors declare that they have no known competing financial interests or personal relationships that could have appeared to influence the work reported in this paper.

Acknowledgments

This work was supported by the EIPHI Graduate School [grant number ANR-17-EURE-0002]; the French Investissements d'Avenir program, project ISITEBFC [grant number ANR-15-IDEX-03]; and the National Natural Science Foundation of China [grant numbers 11732002 and 11672089].

Appendix A. Supplementary data

Supplementary material related to this article can be found online at <https://doi.org/10.1016/j.jmps.2022.104957>.

References

- Abueidda, D.W., Bakir, M., Al-Rub, R.K.A., Bergström, J.S., Sobh, N.A., Jasiuk, I., 2017. Mechanical properties of 3D printed polymeric cellular materials with triply periodic minimal surface architectures. *Mater. Des.* 122, 255–267.
- Berger, J.B., Wadley, H.N.G., McMeeking, R.M., 2017. Mechanical metamaterials at the theoretical limit of isotropic elastic stiffness. *Nature* 543 (7646), 533.
- Blasco, E., Müller, J., Müller, P., Trouillet, V., Schön, M., Scherer, T., Barner-Kowollik, C., Wegener, M., 2016. Fabrication of conductive 3D gold-containing microstructures via direct laser writing. *Adv. Mater.* 28 (18), 3592–3595.
- Bonatti, C., Mohr, D., 2017. Large deformation response of additively-manufactured FCC metamaterials: From octet truss lattices towards continuous shell mesostructures. *Int. J. Plast.* 92, 122–147.
- Bonatti, C., Mohr, D., 2019. Smooth-shell metamaterials of cubic symmetry: anisotropic elasticity, yield strength and specific energy absorption. *Acta Mater.* 164, 301–321.

- Bückmann, T., Schittny, R., Thiel, M., Kadic, M., Milton, G.W., Wegener, M., 2014. On three-dimensional dilational elastic metamaterials. *New J. Phys.* 16 (3), 033032.
- Bückmann, T., Stenger, N., Kadic, M., Kaschke, J., Frölich, A., Kennerknecht, T., Eberl, C., Thiel, M., Wegener, M., 2012. Tailored 3D mechanical metamaterials made by dip-in direct-laser-writing optical lithography. *Adv. Mater.* 24 (20), 2710–2714.
- Chen, Y., Frenzel, T., Guenneau, S., Kadic, M., Wegener, M., 2020a. Mapping acoustical activity in 3D chiral mechanical metamaterials onto micropolar continuum elasticity. *J. Mech. Phys. Solids* 137, 103877.
- Chen, Y., Frenzel, T., Zhang, Q., Kadic, M., Wegener, M., 2021. Cubic metamaterial crystal supporting broadband isotropic chiral phonons. *Phys. Rev. Mater.* 5 (2), 025201.
- Chen, X., Ji, Q., Wei, J., Tan, H., Yu, J., Zhang, P., Laude, V., Kadic, M., 2020b. Light-weight shell-lattice metamaterials for mechanical shock absorption. *Int. J. Mech. Sci.* 169, 105288.
- Chen, Y., Kadic, M., Guenneau, S., Wegener, M., 2020c. Isotropic chiral acoustic phonons in 3D quasicrystalline metamaterials. *Phys. Rev. Lett.* 124 (23), 235502.
- Chen, X., Moughames, J., Ji, Q., Martínez, J.A.I., Tan, H., Adrar, S., Laforge, N., Cote, J.-M., Euphrasie, S., Ulliac, G., Kadic, M., Laude, V., 2020d. Optimal isotropic, reusable truss lattice material with near-zero Poisson's ratio. *Extreme Mech. Lett.* (ISSN: 2352-4316) 41, 101048. <http://dx.doi.org/10.1016/j.eml.2020.101048>.
- Chen, X.Y., Tan, H.F., 2018. An effective length model for octet lattice. *Int. J. Mech. Sci.* 140, 279–287.
- Christensen, R.M., 1986. Mechanics of low density materials. *J. Mech. Phys. Solids* 34 (6), 563–578.
- Cote, F., Deshpande, V., Fleck, N., Evans, A., 2004. The out-of-plane compressive behavior of metallic honeycombs. *Mater. Sci. Eng. A* 380 (1–2), 272–280.
- Coulais, C., Sabbadini, A., Vink, F., van Hecke, M., 2018. Multi-step self-guided pathways for shape-changing metamaterials. *Nature* 561 (7724), 512–515.
- Deshpande, V.S., Ashby, M.F., Fleck, N.A., 2001a. Foam topology: Bending versus stretching dominated architectures. *Acta Mater.* 49 (6), 1035–1040.
- Deshpande, V.S., Fleck, N.A., Ashby, M.F., 2001b. Effective properties of the octet-truss lattice material. *J. Mech. Phys. Solids* 49 (8), 1747–1769.
- Deubel, M., Von Freymann, G., Wegener, M., Pereira, S., Busch, K., Soukoulis, C.M., 2004. Direct laser writing of three-dimensional photonic-crystal templates for telecommunications. *Nature Mater.* 3 (7), 444–447.
- Dragonì, E., Ciace, V.A., 2019. Mechanical design and modelling of lightweight additively manufactured lattice structures evolved from regular three-dimensional tessellations. *Proc. Inst. Mech. Eng. C* 0954406219885959.
- Duan, S., Tao, Y., Lei, H., Wen, W., Liang, J., Fang, D., 2018. Enhanced out-of-plane compressive strength and energy absorption of 3D printed square and hexagonal honeycombs with variable-thickness cell edges. *Extreme Mech. Lett.* 18, 9–18.
- Eberl, C., Thompson, R., Gianola, D., Bundschuh, S., 2006. Digital image correlation and tracking with matlab. *Matlab Central File Exchange*.
- Elsayed, M.S., Pasini, D., 2010. Multiscale structural design of columns made of regular octet-truss lattice material. *Int. J. Solids Struct.* 47 (14–15), 1764–1774.
- Florijn, B., Coulais, C., van Hecke, M., 2014. Programmable mechanical metamaterials. *Phys. Rev. Lett.* 113 (17), 175503.
- Frenzel, T., Findeisen, C., Kadic, M., Gumbsch, P., Wegener, M., 2016. Tailored buckling microlattices as reusable light-weight shock absorbers. *Adv. Mater.* 28 (28), 5865–5870.
- Frenzel, T., Kadic, M., Wegener, M., 2017. Three-dimensional mechanical metamaterials with a twist. *Science* 358 (6366), 1072–1074.
- Frenzel, T., Köpfler, J., Jung, E., Kadic, M., Wegener, M., 2019. Ultrasound experiments on acoustical activity in chiral mechanical metamaterials. *Nature Commun.* 10 (1), 1–6.
- Gibson, L.J., Ashby, M.F., 1999. *Cellular Solids: Structure and Properties*. Cambridge University Press.
- Gümrük, R., Mines, R.A.W., 2013. Compressive behaviour of stainless steel micro-lattice structures. *Int. J. Mech. Sci.* 68, 125–139.
- He, Z., Wang, F., Zhu, Y., Wu, H., Park, H.S., 2017. Mechanical properties of copper octet-truss nanolattices. *J. Mech. Phys. Solids* 101, 133–149.
- Jang, D., Meza, L.R., Greer, F., Greer, J.R., 2013. Fabrication and deformation of three-dimensional hollow ceramic nanostructures. *Nature Mater.* 12 (10), 893–898.
- Kadic, M., Bückmann, T., Stenger, N., Thiel, M., Wegener, M., 2012. On the practicability of pentamode mechanical metamaterials. *Appl. Phys. Lett.* 100 (19), 191901.
- Karathanasopoulos, N., Dos Reis, F., Diamantopoulou, M., Ganghoffer, J.-F., 2020. Mechanics of beams made from chiral metamaterials: Tuning deflections through normal-shear strain couplings. *Mater. Des.* 189, 108520.
- Knowles, K.M., Howie, P.R., 2015. The directional dependence of elastic stiffness and compliance shear coefficients and shear moduli in cubic materials. *J. Elasticity* 120 (1), 87–108.
- Li, T., Jarrar, F., Al-Rub, R.A., Cantwell, W., 2021. Additive manufactured semi-plate lattice materials with high stiffness, strength and toughness. *Int. J. Solids Struct.* 111153.
- Meyers, M.A., Chawla, K.K., 2008. *Mechanical Behavior of Materials*. Cambridge University Press.
- Meza, L.R., Das, S., Greer, J.R., 2014. Strong, lightweight, and recoverable three-dimensional ceramic nanolattices. *Science* 345 (6202), 1322–1326.
- Meza, L.R., Philpot, G.P., Portela, C.M., Maggi, A., Montemayor, L.C., Comella, A., Kochmann, D.M., Greer, J.R., 2017. Reexamining the mechanical property space of three-dimensional lattice architectures. *Acta Mater.* 140, 424–432.
- Milton, G.W., Cherkav, A.V., 1995. Which elasticity tensors are realizable? *J. Eng. Mater. Technol.* 117 (4), 483–493.
- Mizzi, L., Spaggiari, A., 2020. Lightweight mechanical metamaterials designed using hierarchical truss elements. *Smart Mater. Struct.* 29 (10), 105036.
- Queheillalt, D.T., Wadley, H.N., 2005. Cellular metal lattices with hollow trusses. *Acta Mater.* 53 (2), 303–313.
- Schittny, R., Kadic, M., Bückmann, T., Wegener, M., 2014. Invisibility cloaking in a diffusive light scattering medium. *Science* 345 (6195), 427–429.
- Tan, X., Chen, S., Wang, B., Tang, J., Wang, L., Zhu, S., Yao, K., Xu, P., 2020. Real-time tunable negative stiffness mechanical metamaterial. *Extreme Mech. Lett.* 41, 100990.
- Tan, X., Chen, S., Wang, B., Zhu, S., Wu, L., Sun, Y., 2019a. Design, fabrication, and characterization of multistable mechanical metamaterials for trapping energy. *Extreme Mech. Lett.* 28, 8–21.
- Tan, X., Chen, S., Zhu, S., Wang, B., Xu, P., Yao, K., Sun, Y., 2019b. Reusable metamaterial via inelastic instability for energy absorption. *Int. J. Mech. Sci.* 155, 509–517.
- Tan, X., Wang, B., Zhu, S., Chen, S., Yao, K., Xu, P., Wu, L., Sun, Y., 2019c. Novel multidirectional negative stiffness mechanical metamaterials. *Smart Mater. Struct.* 29 (1), 015037.
- Tancogne-Dejean, T., Diamantopoulou, M., Gorji, M.B., Bonatti, C., Mohr, D., 2018. 3D plate-lattices: An emerging class of low-density metamaterial exhibiting optimal isotropic stiffness. *Adv. Mater.* 30 (45), 1803334.
- Tancogne-Dejean, T., Mohr, D., 2018a. Elastically-isotropic elementary cubic lattices composed of tailored hollow beams. *Extreme Mech. Lett.* 22, 13–18.
- Tancogne-Dejean, T., Mohr, D., 2018b. Stiffness and specific energy absorption of additively-manufactured metallic BCC metamaterials composed of tapered beams. *Int. J. Mech. Sci.* 141, 101–116.
- Tancogne-Dejean, T., Spierings, A.B., Mohr, D., 2016. Additively-manufactured metallic micro-lattice materials for high specific energy absorption under static and dynamic loading. *Acta Mater.* 116, 14–28.
- Tao, Q., Wang, C., Wang, K., Xie, Z., Tan, H., 2020. Mixed-mode bending of a smart reconfigurable lattice structure with bi-directional corrugated core. *Int. J. Mech. Sci.* 105848.
- Ushijima, K., Cantwell, W.J., Mines, R.A.W., Tsoupanos, S., Smith, M., 2011. An investigation into the compressive properties of stainless steel micro-lattice structures. *J. Sandw. Struct. Mater.* 13 (3), 303–329.
- Yang, H., Ma, L., 2020. 1D to 3D multi-stable architected materials with zero Poisson's ratio and controllable thermal expansion. *Mater. Des.* 188, 108430.

- Zheng, X., Lee, H., Weisgraber, T.H., Shusteff, M., DeOtte, J., Duoss, E.B., Kuntz, J.D., Biener, M.M., Ge, Q., Jackson, J.A., et al., 2014. Ultralight, ultrastiff mechanical metamaterials. *Science* 344 (6190), 1373–1377.
- Zhu, S., Tan, X., Wang, B., Chen, S., Hu, J., Ma, L., Wu, L., 2019. Bio-inspired multistable metamaterials with reusable large deformation and ultra-high mechanical performance. *Extreme Mech. Lett.* 32, 100548.
- Zok, F.W., Latture, R.M., Begley, M.R., 2016. Periodic truss structures. *J. Mech. Phys. Solids* 96, 184–203.